

# Stellar metallicity of star-forming galaxies at $z \sim 3$ \*

Veronica Sommariva<sup>1</sup>, Filippo Mannucci<sup>1,2</sup>, Giovanni Cresci<sup>1</sup>, Roberto Maiolino<sup>3</sup>, Alessandro Marconi<sup>4</sup>,  
Tohru Nagao<sup>5</sup>, Andrea Baroni<sup>4</sup>, and Andrea Grazian<sup>3</sup>

<sup>1</sup> INAF-Osservatorio Astrofisico di Arcetri, Firenze, Italy

\*\* e-mail: [veronica@arcetri.astro.it](mailto:veronica@arcetri.astro.it)

<sup>2</sup> Harvard-Smithsonian Center for Astrophysics, 60 Garden street, Cambridge, MA 02138, USA

<sup>3</sup> INAF-Osservatorio Astronomico di Roma, Monte Porzio Catone, Italy

<sup>4</sup> Dipartimento di Astronomia, Università di Firenze, Firenze Italy

<sup>5</sup> Kyoto University, Japan

Received 22-09-11; accepted 09-12-11

## ABSTRACT

The stellar metallicity is a direct measure of the amount of metals present in a galaxy, as a large part of the metals lie in its stars. In this paper we investigate new stellar metallicity indicators suitable for high- $z$  galaxies studying the stellar photospheric absorption lines in the rest frame ultraviolet, hence sampling predominantly young hot stars. We defined these new indicators based on the equivalent widths (EW) of selected features using theoretical spectra created with the evolutionary population synthesis code *Starbursts99*. We used them to compute the stellar metallicity for a sample of UV-selected galaxies at  $z > 3$  from the AMAZE survey using very deep (37h per object) VLT/FORS spectra. Moreover, we applied the new metallicity indicators to eight additional high redshift galaxies found in literature. We then compared stellar and gas-phase metallicities measured from the emission lines for all these galaxies, finding that within the errors the two estimates are in good agreement, with possible tendency to have stellar metallicities lower than the gas phase ones. For the first time, we are able to study the stellar mass-metallicity relation at  $z > 3$ . We find that the metallicity of young, hot stars in galaxies at  $z \sim 3$  have similar values of the aged stars in local SDSS galaxies, contrary to what observed for the gas phase metallicity.

**Key words.** galaxies: evolution – galaxies:high-redshift

## 1. Introduction

Metallicity is one of the important properties of galaxies, and its study is able to shed light on the details of galaxy evolution. It is, in fact, an integrated property, related to the whole past history of the galaxies. In particular, metallicity is sensitive to whole star formation history, and so to evolutionary stage of the galaxy. Moreover, it is affected by presence of infalls and outflows, i.e. by feedback processes and by the interplay between the forming galaxy and the intergalactic medium (see e.g. Erb et al. 2008, Mannucci et al. 2009, Cresci et al. 2010). As consequence, it has become an important test of galaxy evolution (e.g. Nagamine et al. 2001, Spitoni et al. 2010, Davè et al. 2011).

Local galaxies show a clear correlation between mass and metallicity (MZR), for which the galaxies with larger stellar mass have higher metallicities, and this correlation appears to hold both in term of gas-phase metallicity (e.g. Tremonti et al. 2004) and stellar metallicity (Gallazzi et al. 2005, Panter et al. 2008).

At high-redshift the gas-phase metallicity of the ISM of star-forming galaxies has been measured using primarily

oxygen abundances. The most common techniques to determine the gas phase metallicity are based either on theoretical calibrations (see Kewley & Ellison 2002, and Kewley & Ellison 2008) or on empirical metallicity calibrations, the so-called “strong line diagnostics”, which are based on the ratios of collisionally excited forbidden lines to hydrogen recombination lines. Previous studies have shown that the mass-gas phase metallicity relation presents evidence of strong redshift evolution. Among others, Savaglio et al. (2005) and Zahid et al. (2011) studied star forming galaxies at redshift  $z \sim 0.7$  and demonstrated that, at given mass, these galaxies shown lower metallicity than the SDSS sample at  $z \sim 0.1$ . Erb et al. (2006) reported a more significant decrease of metallicity in galaxies at  $z \sim 2.2$ . Two projects were specifically designed to extend the investigation of MZR at  $z > 3$ : LSD (Lyman-break Stellar population and Dynamic) and AMAZE (Assessing the Mass-Abundance redshift Evolution). With these projects, Maiolino et al. (2008) and Mannucci et al. (2009) showed for the first time the evolution of the mass-metallicity relation at  $z > 3$ . However, the redshift evolution of the gas phase metallicity in galaxies have been questioned recently by Mannucci et al. (2010). They discovered that metallicity depends not only on the mass, but also from the Star Formation Rate (SFR): for a given stellar mass, galaxies with higher SFRs systematically show lower metallicities. This is the

\* Based on ESO observations, proposals 082.A-0398 and 084.A-0367

\*\*

so-called “Fundamental Metallicity Relation (FMR)”, i.e., a tight relation between stellar mass, gas-phase metallicity, and star formation rate (SFR). Local SDSS galaxies show very small residuals around this relation, of the order of 0.05dex. Yates et al. (2011) found a similar relation, with some differences due to the metallicity calibration adopted. According to Mannucci et al. (2010), the FMR does not appear to evolve with redshift up to  $z \sim 2.5$ , with the high redshift galaxies following the same FMR defined by the local SDSS galaxies. This suggests that the observed evolution of the mass-metallicity relation is due to selection effects and to the increase of the average SFR with redshift. In fact, the measured metallicity in several additional samples of high- $z$  galaxies results to be in agreement with the predictions of the FMR given the mass and SFR of the galaxies: galaxies having lower SFRs than the general population at their redshifts also have higher metallicities (e.g., Richard et al. 2011, Nakajima et al. 2011), and galaxies with higher SFRs also have lower metallicities (e.g., Erb et al. 2010, Contini et al. 2011, Sanders et al. 2011), so that all these galaxies follow the FMR. Also, the FMR allowed Mannucci et al. 2011 and Campisi et al. 2011 to show that the hosts of the long- GRBs have the same metallicity properties of the other star-forming galaxies. However, they found some metallicity evolution of the FMR at  $z \sim 3.3$ , where galaxies tend to have lower metallicities.

All the observational studies mentioned in the previous paragraph refer to the gas-phase metallicity, as measured by emission lines. Gallazzi et al. (2005) presented the local mass-stellar metallicity relation based on  $\sim 170000$  SDSS galaxies (Sloan Digital Sky Survey Data Release Two). The stellar metallicities were derived using the Lick system of spectral indices in the optical region which are sensitive to the overall metallicity of the stellar population, primarily dominated by intermediate/old stars. They adopted a Bayesian statistical approach and derived the stellar metallicities by comparing the observed spectrum of each galaxy with a comprehensive library of model spectra corresponding to different star formation histories. They found that at low masses, the stellar metallicity increase with mass, while above  $\sim 3 \times 10 M_{\odot}$  the relation flattens out. In addition they noted that gas-phase metallicity is best determined for star-forming galaxies, whereas stellar metallicity is best determined for early-type galaxies, and found that the stellar metallicity is generally lower than the gas-phase metallicity (by 0.5 dex). More recently Panter et al. (2008) inferred the stellar metallicity history of SDSS galaxies and determined their stellar mass-metallicity relation. They used a different approach respect to Gallazzi et al. (2005), but they found similar results. Moreover, considering only the younger population of galaxies ( $\leq 1$  Gyr) they found good agreement also with the gas phase metallicities.

A very limited work has instead been done on stellar metallicity at high redshift, see Shapley (2011) for a recent review. As in local *starbursts*, the strongest features in the rest-frame UV spectrum of distant galaxies are interstellar and photospheric absorption lines of C, N, O, Si, and Fe, produced by hot, young O-B stars (see Shapley et al. 2003). One advantage in using these spectra to measure the metallicity at  $z \sim 3$  is that the UV rest frame is shifted into the optical spectral region, which is easier to observe

from the ground-based telescope. However, very high signal to noise on the stellar continuum is required to study the relevant absorption features for metallicity measurements, and therefore such studies were obtained, until now, mainly for gravitationally lensed galaxies (Rix et al. 2004, Quider et al. 2009, Dessauges-Zavadsky et al. 2010) or for co-added star forming galaxy spectra (Halliday et al. 2008).

Several authors have presented calibrations for stellar metallicity based on UV absorption lines. Leitherer et al. (2001) investigated the influence of metallicity on the spectra of star forming galaxies. In particular, they investigated the existence of some blended photospheric lines whose strengths depend on metallicities only. They found that the two blends of lines near  $\lambda 1370$  and  $\lambda 1425$  (which they attributed to OV  $\lambda 1371$  and FeV  $\lambda 1360$ - $\lambda 1380$  and to  $\lambda$ SiIII  $\lambda 1417$ , CIII  $\lambda 1427$  and FeV  $\lambda 1430$  respectively) have equivalent widths that increase steadily with metallicity and do not depend on other stellar parameters, as age and IMF. Rix et al. (2004) using the *Starburst99* plus their non-LTE model atmosphere code WM-basic, supported the conclusions that these lines are useful metallicity indicators, and suggested a new indicator at  $\lambda 1978$ . Rix et al. (2004) applied the new indicators to measure the stellar metallicity of two lensed galaxies, MS 1512-cB58 at  $z=2.73$ , and Q1307-BM1163 at  $z=1.411$ , finding good agreement with the gas phase metallicity.

On the basis of these works, Mehelert et al. (2006) calculated the EWs of the  $\lambda 1370$   $\lambda 1425$  for 12 galaxies with  $2.37 < z < 3.40$  in the FORS deep field. They investigated the evolution of the EWs and the metallicity with the redshift, and found that the abundances of heavy elements is increasing between  $z \sim 0.5$  and  $z \sim 2.5$ . Halliday et al. (2008), instead, computed the stellar metallicity using the  $\lambda 1978$  indicator for a co-added unlensed star forming galaxies spectra at  $z \sim 2$ . Comparing their results with the gas phase metallicity of galaxies with similar mass, they found that their stellar metallicities were lower by a factor of  $\sim 0.25$ dex. Quider et al. (2009) computed the stellar metallicity for the gravitationally lensed galaxies Cosmic Horseshoe at  $z = 2.38$  by using the  $\lambda 1425$  metallicity indicator, found good agreement between stellar and gas phase metallicity. More recently, Quider et al. (2010) carried on the same work for the lensed galaxies Cosmic Eye at  $z = 3.07$ . Because of the presence a strong sky lines in the region of the stellar metallicity indicators, they do not give the exact value of the stellar metallicity, but just an indication by comparing the observed spectra with the model. Finally, Dessauges-Zavadsky et al. (2010) studied the stellar metallicity for the lensed galaxy 8 o'clock arc at  $z = 2.73$ . Using the  $\lambda 1425$  and  $\lambda 1978$  photospheric indices, they found comparable metallicity for the gas and the stellar component.

All these studies provide important constraints to the models of galaxy formation. In fact, many models study the processes of gas infall and outflows, and the properties of feedback and galactic winds (Dekel & Woo 2003, Veilleux, Cecil & Bland-Hawthorn 2005, Murray, Quataert & Thompson 2005, Davé, Finlator & Oppenheimer 2007, de Rossi, Tissera & Scannapieco 2007, Brooks et al. 2007, Tornatore et al. 2007, Somerville et al. 2008, Oppenheimer & Davé 2008, Finlator & Davé 2008, Mouchine et al.

2008, Dayal et al. 2009, Tassis, Kravtsov & Gnedin 2008, Kobayashi et al. 2007, Calura et al. 2009, Spitoni et al. 2010, Salvaterra et al. 2010, Sakstein et al. 2011). The no evolution of the FMR, the associated evolution of the mass-metallicity relation, and the properties of the effective yields put strong constraint on them. In this picture, the stellar metallicity can be used as independent measurement to test the predicted metallicity evolution (De Rossi et al. 2007, Davé & Oppenheimer 2007).

In this work we study the stellar metallicity of a sample of galaxies at  $z > 3$ .

In the next section we review the different indices used for stellar metallicity estimates at high- $z$ , and define new rest frame UV feature suitable for such measurements to enlarge the number of available metallicity indicators. In Section 3 we present our sample of high redshift galaxies and we compute their stellar metallicity applying the calibrations found. In Section 4 we calculate the stellar and gas phase metallicity for some lensed galaxies found in literature, and we compare the two. Finally we present the first stellar mass-metallicity relation obtained at  $z > 3$ , followed by the conclusions.

## 2. Stellar metallicity from absorption lines

When studying high-redshift galaxies, is useful to have a large number of calibrated features over a large wavelength range to increase the constraints on metallicity and avoid the effects of atmospheric absorption bands and bright sky emission lines.

A feature can be used as a metallicity indicator if the following conditions are satisfied: 1) the EW is deep enough to be measured in high redshift galaxies; 2) it varies significantly with the metallicity; and 3) it does not depends critically on age or IMF.

The aim of this work is to update the old metallicity calibrations and to enlarge the number of indices over all the range of UV spectral region.

We want measure the stellar metallicities of high redshift galaxies by comparing the observed photospheric lines to the results of the population synthesis code *Starbursts99* (Leitherer et al. 1999). The original version of this code allowed the creation of synthetic UV spectra with a variety of ages and IMFs, and used the stellar evolution models to follow the stellar population over the time. The first release included only few different metallicities because empirical stellar libraries were available only for Milky Way O-type stars observed with the International Ultraviolet Explorer (IUE) satellite. The galactic B stars were later included to that library by de Mello et al. (2000). In order to consider the sub-solar heavy elements abundances, a new improvement was obtained in 2001 with the inclusion of a library of O-type spectra obtained from HST STIS observations of stars in Large and Small Magellanic Clouds (Leitherer et al. 2001). Rix et al. (2004) followed an other approach by utilizing theoretical library spectra instead than empirical ones. Their purpose was synthesized the photospheric absorption lines seen in the spectra of star forming galaxies taking into account on the non-LTE model atmosphere, the stellar wind and their effects in the spectral synthesis of hot stars. Therefore they replaced the empirical library with a grid of theoretical spectra generated with the hydrodynamics code WM-basic. The major difference between this two

**Table 1.** List of the metallicity indicators with the corresponding elements, and regions where the equivalent widths are integrated. For an additional indicator at  $\lambda 1533$  see sec. 2.4

Indicator ID	element	$\lambda$ range
F1370	OV, FeV	1360–1380 <sup>a</sup>
F1425	CIII, FeV, SiIII	1415–1435 <sup>a</sup>
F1460	NiII	1450–1470 <sup>b</sup>
F1501	SV	1496–1506 <sup>b</sup>
F1978	FeIII	1935–2020 <sup>c</sup>

**Notes.** <sup>(a)</sup> Leitherer et al. 2001 <sup>(b)</sup> this work <sup>(c)</sup> Rix et al.2004.

approaches is that the empirical spectra include prominent UV interstellar absorption lines not present in the theoretical spectra, which are purely stellar. Nevertheless, they found good agreement between the empirical and the theoretical spectra.

Because Rix et al. (2004) in principle focus on photospheric lines, processes such as shock emission that affect only the high-ionization wind lines were not included in their models. These limitations have been addressed to some extent in the latest generation of the WM-basic code (Leitherer et al. 2010), which is used in this work. The latest generation of the WM-basic code is optimized to compute the strong P Cygni type lines originating in the wind of the hot stars. This is a great advantage respect use only the faint photospheric lines, because the stellar-wind features are stronger, therefore more easy to detect in low S/N spectrum.

*Starburst99* with the WM-basic library allows the creation of simulated spectra depending on a number of free parameters related to star formation history, IMF, age, metallicity, supernova and black hole cut-off, stellar atmospheres and microturbulence. We generated galaxy model spectra using the Padova tracks, with thermally pulsing AGB stars added, for five values of metallicities, 0.02, 0.4, 0.2, 1.0 and 2.5  $Z_{\odot}$ , and assuming continuous star formation histories, results in Fig. 1 We considered five different stellar initial mass function (IMF). The reference model is a classical Salpeter power law with exponent  $\alpha = 2.35$  and upper mass limit  $M_{up} = 100M_{\odot}$ . We also considered IMFs with  $\alpha = 1.85$  and  $\alpha = 2.85$  between  $1M_{\odot}$  and  $100M_{\odot}$ , and with  $\alpha = 2.35$  and mass limit  $M_{up} = 60M_{\odot}$ . Finally, we compute models using the Kroupa IMF.

### 2.1. Metallicity indicators

The UV spectrum of star forming galaxies is dominated by strong photospheric absorption features that are sensitive to metallicity.

Leitherer et al. (2001) investigated the existence of some blended photospheric lines whose strengths depend on metallicities only. They found that the two blends of lines near  $\lambda 1370$  and  $\lambda 1425$  (which they attributed to OV  $\lambda 1371$  and FeV  $\lambda 1360$ – $\lambda 1380$  and to  $\lambda$ SiIII 1417, CIII  $\lambda 1427$  and FeV  $\lambda 1430$  respectively) have equivalent widths that increase steadily with metallicity and do not depend on other parameters. Rix et al. (2004) supported the conclusions that these lines are useful metallicity indicators, and suggested a new robust indicator at  $\lambda \sim 1978 \text{ \AA}$ .

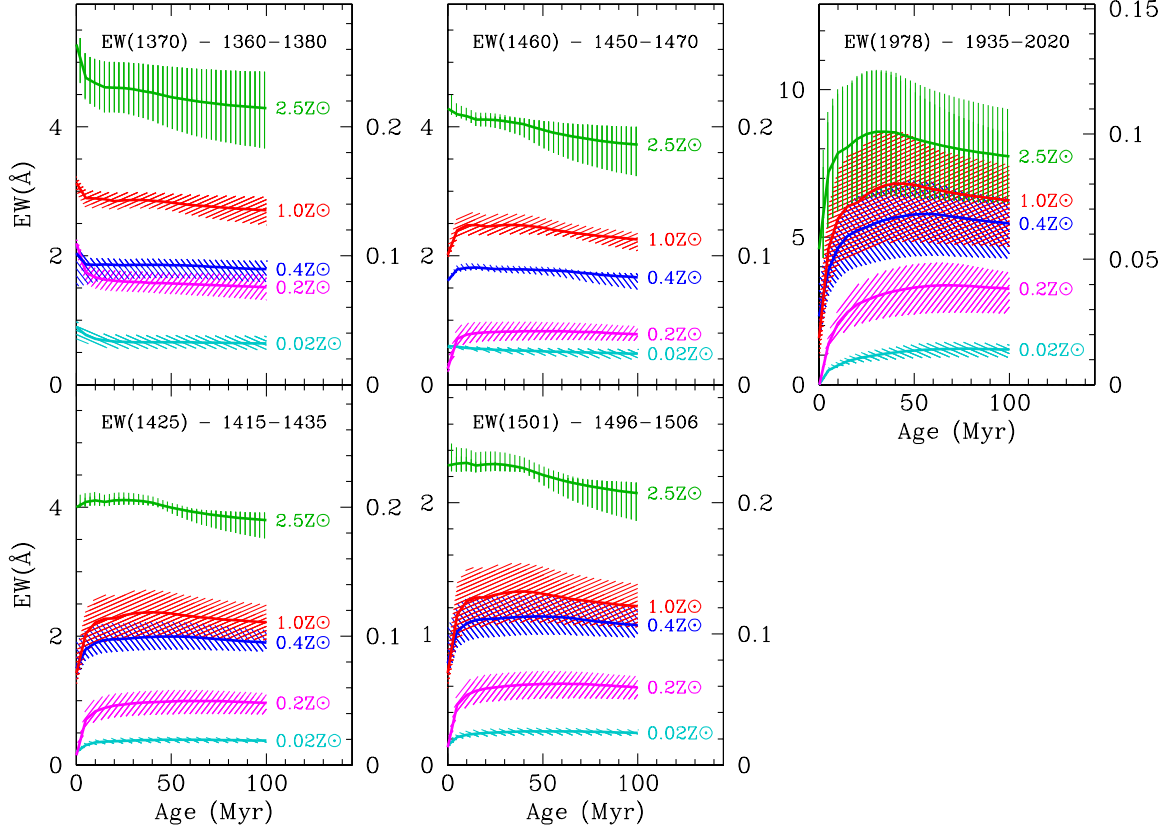


**Fig. 1.** Variation of the line indices with stellar population age and metallicity. In each plot, the EW is shown in left vertical axis, while the right axis shows the average fractional depth below the continuum. For each feature we draw the models constructed with *Starburst99* at five value of metallicity as shown in different colors. For each metallicity, the color regions represent the error due to the dependence on the IMF assumed. In this way we can highlight the dependence of the models and robustness of the indices from the IMF and stellar population age assumed.

Here we use the spectra of the new version of *Starburst99* to update the calibrations of the features mentioned above and find additional new useful features. Using the new library, our measurements confirm that the indicators proposed in the previous studies, (F1370, F1425, and F1978), are stable after  $\sim 30\text{Myr}$  from the onset of star formation, and increase monotonically with the metallicity with mild dependence on other parameters (see Fig. 1). Previous works have successfully used these indices (Halliday et al. 2008 and Quider et al. 2009). The predicted EWs derived using the last version of the *Starburst99* code are similar from the previously ones used for the 1425 index ( $0.11\text{\AA}$  at solar metallicity). However for the 1978 index the difference is higher, especially at high metallicity ( $1.95\text{\AA}$  at solar metallicity). Moreover, the F1978 index is quite sensitive to the assumed IMF (see Fig. 3), making it more uncertain among the metallicity indicator.

## 2.2. New indicators

The first region that we investigate is between 1496 and  $1506\text{\AA}$ . We choose this region because the SV  $\lambda 1501$  line is an absorption feature that arise in the photosphere of

the hot stars, as Pettini et al. (1999) and Quider et al. (2009) mentioned. Fig. 1 shows the age stability and the dependence on metallicity of this index: as for the previous cases, this line satisfies the necessary conditions to be used as indicator.

Another region that we consider is between 1450 and  $1470\text{\AA}$ . No one mentioned before this region for some photospheric lines, but we found that the NiII at  $\lambda 1460$  feature has the same behavior of the other lines discussed above, with the equivalent width depending strongly on the metallicity, but not on age and IMF. We therefore defined two new line indices, F1460, and F1501, as the equivalent widths integrated between  $1450\text{--}1470\text{\AA}$  and  $1496\text{--}1506\text{\AA}$  respectively.

The list of the metallicity indicators presented above are reported in Tab. 1. Fig. 2 presents the smoothed and normalized reference models obtained with *Starburst99* at metallicity 0.02, 0.4, 0.2, 1, and  $2.5Z_{\odot}$ . The strengths of the absorption features discussed above is clearly a strong and monotonic function of metallicity.

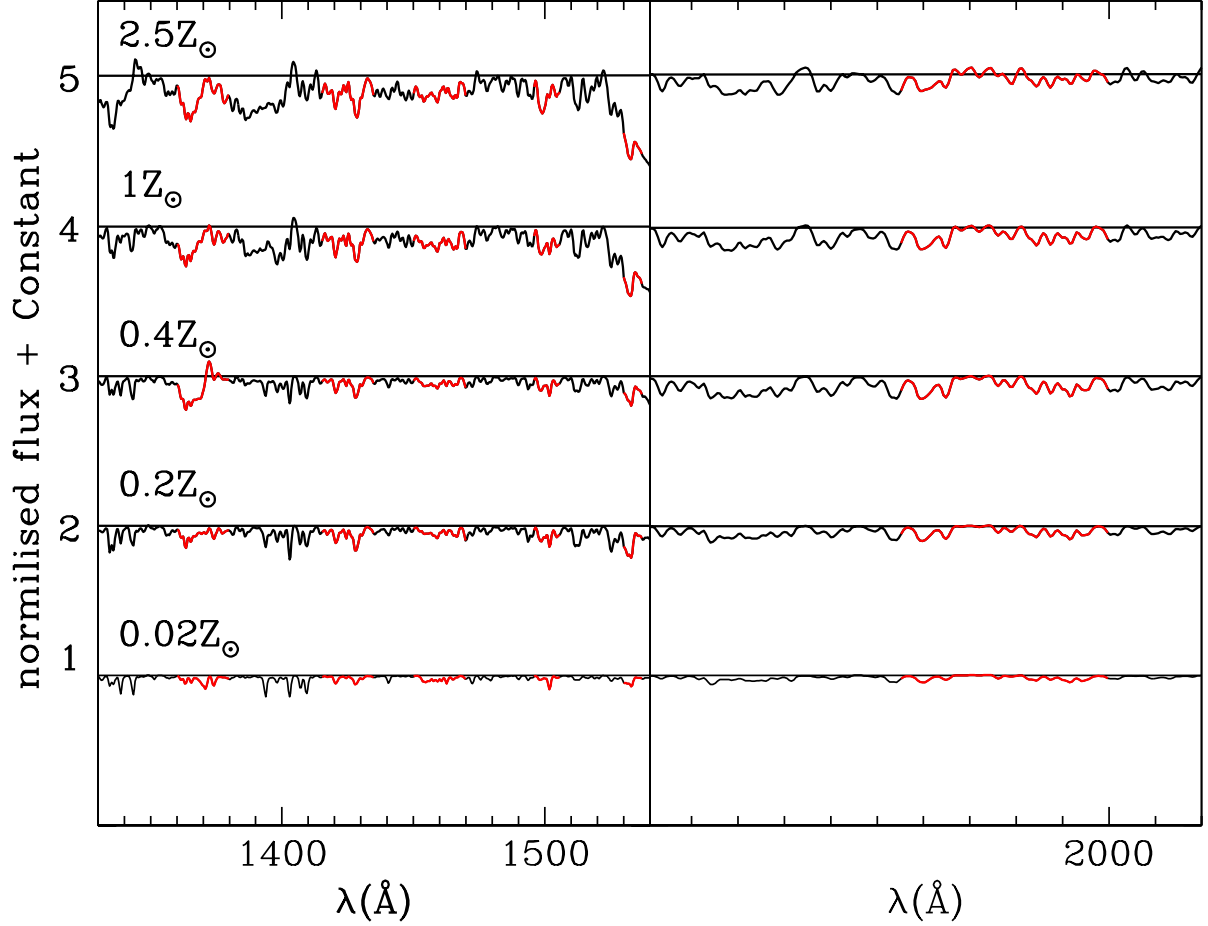


**Fig. 2.** Smoothed and normalized reference models obtained with *Starbursts99* at metallicity 0.02, 0.4, 0.2, 1 and  $2.5Z_{\odot}$ . In red are highlighted the metallicity indicators discussed in the text to show their dependence from metallicity.

### 2.3. Metallicities calibrations

For an accurate determination of metallicity, we interpolate the relation between the equivalent widths of the indicators as a function of  $\text{Log}(Z/Z_{\odot})$  discussed above.

We fitted a second-order polynomial to measured the values of the equivalent widths. The results of the fitting is presented in Fig. 3: the triangles represent the reference model (Salpeter IMF with  $\alpha = 2.35$  and age=50 Myr), the black line is the quadratic fit of these models, and the grey region represents the uncertainty on the calibration due to the different IMF assumed, as shown in Fig. 1.

We use a second-order fit expressed as:

$$\log(Z/Z_{\odot}) = \alpha + \beta EW + \gamma EW^2 \quad (1)$$

The coefficients for the five indices are in Table 2.

### 2.4. The feature Sill at 1533Å

In addition to the two new indicators found, we also studied the SiII  $\lambda 1533$  feature, defined as the EWs integrated between 1530 and 1537 Å. This line seems to work very well as indicator: apart from satisfying the necessary conditions to consider it as good index (as discussed in Sec. 2.2), this line is in fact very deep respect to the others and defined in narrow wavelength range of 7 Å.

**Table 2.** Coefficient of the equation  $\text{Log}(Z/Z_{\odot}) = \alpha + \beta EW + \gamma EW^2$  for each index considering the real continuum.

Index	$\alpha$	$\beta$	$\gamma$
F1370	-2.501	1.403	-0.1700
F1425	-2.003	1.203	-0.1521
F1460	-2.023	1.251	-0.1631
F1501	-2.152	2.324	-0.5329
F1978	-2.051	0.388	-0.0122

**Table 3.** Coefficient of the equation  $\text{Log}(Z/Z_{\odot}) = \alpha + \beta EW + \gamma EW^2$  for each index, considering the pseudo continuum.

Index	$\alpha$	$\beta$	$\gamma$
F1370	-2.897	2.346	-0.4208
F1425	-2.138	2.116	-0.4424
F1460	-2.183	2.336	-0.5212
F1501	-2.543	4.800	-1.968
F1978	-2.774	1.070	-0.0936

Unfortunately, the SiII is often detected also in emission: see e.g. the very high signal to noise ratio spectrum presented by Shapley et al. (2003). This emission appears to be very weak, and in low resolution spectra it may diffi-

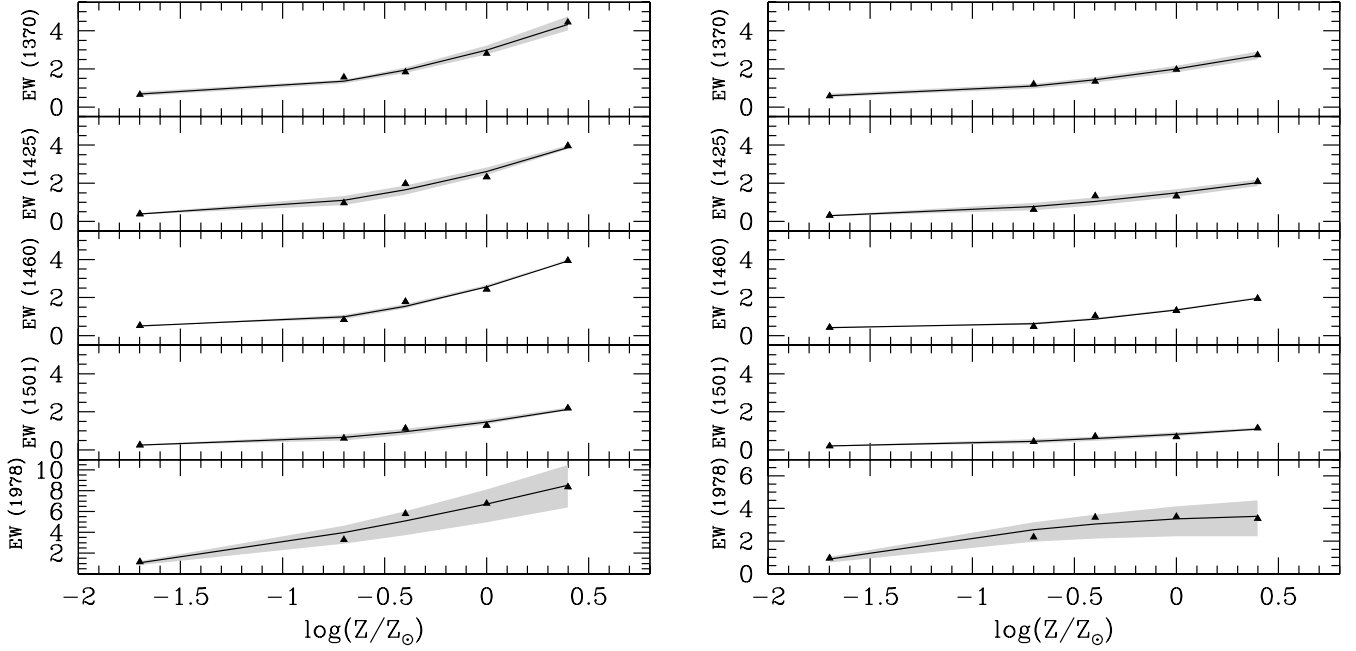


**Fig. 3.** EW-Z relations for the five indices considered. The triangles represent equivalent widths measured from the reference models at age 50 Myr, while the solid line is the quadratic fit given by equations in Table 2 for the real continuum (left panels) and Table 3 for the “pseudo-continuum” (right panels). The grey region represents the error due to the dependence of the models on the IMF assumed.

cult to recognize it. In addition, this is a fine line structure, (Pettini et al. 2004): although this feature is normally photospheric, in dense environments it can be interstellar as well. Therefore we suggest to use it with caution, and only in the spectra where this emission is absent or weak enough to not compromise the measurements of the EW.

We nevertheless present the calibrations obtained for this feature, and discuss the results found for the observed galaxies using it as metallicity indicator.

The obtained calibrations are:

$$\text{Log}(Z/Z_{\odot}) = -1.845 + 1.332EW - 0.2077EW^2 \quad (2)$$

in the case of real continuum, and

$$\text{Log}(Z/Z_{\odot}) = -1.893 + 1.717EW - 0.339EW^2 \quad (3)$$

in case of “pseudo-continuum”.

The results found using this feature are in Sec. 3.4.

### 2.5. Calibration uncertainties

In previous sections we defined two new photospheric lines sensitive to stellar metallicity and independent to the other stellar parameter (such as age and IMF),  $\sim 1460\text{\AA}$  and  $\sim 1501\text{\AA}$ , and we recalibrate with updated stellar libraries the stellar features at  $\sim 1370\text{\AA}$   $\sim 1425\text{\AA}$  and at  $\sim 1978\text{\AA}$  proposed by Leitherer et al. (2001) and Rix et al. (2004) to derive the stellar metallicity.

Both the old and the new metallicity indicator suffer of significant uncertainties.

*Starbursts99* consider two different cases of star formation: an instantaneous burst and a continuous star formation at constant rate: in the former the spectrum changes rapidly with time, in the latter the equilibrium is reached after few

Myr, and then the spectrum changes little with the time. In case of one single burst we expect to observe galaxies where the O-B stars are already died, however galaxies with continuous star formation rate are dominated by bright and hot massive stars which determine the UV continuum (see Adelberger et al. 2004). Therefore, we decided to consider the continuous star formation rate to create models with *Starbursts99* because it seems to be the better description for most star forming galaxies.

Another critical issue in this kind of work is the determination of the continuum. It is worth noticing that, unlike what was done in other similar works (see Rix et al. 2004) the values of EW are relative to the real, theoretical continuum. However, often low- and medium resolution spectra do not have many spectral regions free from absorption lines, and the estimate of such a continuum is not straightforward. For this reason it is common to define a “pseudo” continuum: this is derived by fitting a spline curve through the mean flux in some spectral windows relatively free from emission and absorption lines, and a normalized spectrum is obtained dividing by this fit. This definition tends to underestimate the real continuum because no spectral window is totally free from absorptions, but using the same definition of “pseudo” continuum for both calibrations and observations, this uncertainty tends to cancel out.

When observing faint, high-redshift galaxies, this method is difficult to use, either because not enough signal-to-noise ratio is present in the narrow wavelength ranges ( $1-2\text{\AA}$ , Rix et al. 2004) used to define the “pseudo” continuum, or because bright sky-lines present at  $\lambda > 7000\text{\AA}$  can mask these regions. As a consequence, each spectrum needs different recipe to compute the continuum according to the wavelength range covered and to the signal-to-noise ratio in each point. Because in some cases it is easier to use the “pseudo”

continuum and in other cases is better to estimate the real continuum, we provide both the calibrations.

The coefficients for the calibrations using the definition of the “pseudo-continuum” by Rix et al. (2004) (see Table 3 in their paper for the regions used to define the continuum) and using the last version of *Starburts99* are in Table 3. Fig. 3 (right panel) show the relations obtained between metallicity and EW.

A side effect of these two different procedures is that these calibrations have no or very weak dependency on spectral resolution, as far it is high enough to well sample the region of interest, i.e.,  $10\text{\AA}$  rest-frame. Only the F1978 index depends strongly on resolution, as already noticed by Halliday et al. (2008). In addition this index depends also on the IMF, as shown Fig. 3.

It is worth noticing that these latter calibrations are more easy to use because the definition of the “pseudo continuum” is unambiguous: in fact only some tiny and defined regions are used to defined the “pseudo continuum”, and not the entire continuum is considered, as in the other case. Therefore, we recommend to use the “pseudo continuum” in case of spectra with high signal-to-noise ratio, where the continuum is less affected by bright sky lines and emission or absorption interstellar lines, and in case of low signal-to-noise spectra we suggest to use the first relations and define the real continuum for each spectrum in order to select regions not affected by strong, bright sky lines.

### 3. Stellar metallicity in high redshift galaxies in the AMAZE sample.

In this section we apply the method and the relations presented above to a sample of five galaxies at  $z \sim 3.3$ , in order to find, for the first, the stellar mass-metallicity relation at this redshift.

#### 3.1. Observations

For the present investigation we selected a sub-sample of AMAZE galaxies at  $z \sim 3.3$  for which gas metallicities and stellar mass were already accurately measured by Maiolino et al. (2008) and Troceno et al. (in preparation, see Table 4). The masses presented in Table 4 are slightly different from those presented in Maiolino et al. (2008) because the calculation was improved by using new Spitzer IRAC photometry available. The observed galaxies have been originally selected in the GOODS-MUSYC sample (Grazian et al. 2006), and are all in same field allowing for multi-object spectroscopy.

Observations of the galaxies were obtained in service mode in three runs (Nov-Dec. 2008, Nov-Dec. 2009 and Sept-Dec. 2010) using FORS2 (FOcal Reduced and low dispersion Spectrograph 2, Appenzeller et al. 1992) at the ESO VLT (UT4), under seeing conditions of about 0.8 for each run. The extended multi-object mode (MXU) was used to optimize the number and placement of targets in the masks.

To assure a homogeneous sample the observations were carried out using a standardized set-up. The slit width was equally set to 1 arcsec, corresponding approximately to the size of typical high-redshift galaxies under average atmospheric conditions at Paranal. For all observations, the low resolution grism 300I was used. This grism covers a range of the CCD sensitivity (6000 – 11000

$\text{\AA}$ ) with a relatively high efficiency, reaching its maximum at around 8600  $\text{\AA}$ . The total exposure times was 37h.

#### 3.2. Data reduction

The data reduction was performed using the ESO FORS-pipeline. The default reduction of spectroscopic science data is as follows: the data are first corrected for bias, then an extracted mask, containing the positions of the long slit and the spatial curvatures of the spectra, is applied to the science data; they are then flat-fielded and re-mapped eliminating the cosmic-ray and the optical distortions. Afterwards they are rebinned to constant wavelength steps. The wavelength calibration is adjusted using sky emission lines: this allows to correct for shifts between night-time science and day-time calibration data.

The sky background is obtained using a median of the pixel free from emission lines, and the sky is subtracted before remapping, i.e. when the spectra are still in the original CCD coordinate system. The sky is determined with a robust linear fitting, which allows for a linear spatial gradient in the background.

Flux calibration was performed using spectra of spectrophotometric standard stars obtained each night. These spectra were reduced with the pipeline, as for the science data, and used to convert the ADUs into flux units. The observed spectra of the standard stars are divided by the corresponding stellar spectra taken from the literature in order to obtain response curves and calibration factors. Representative correction curves are created for each run combining the individual response curves and smoothing the result by a spline interpolation. Finally we applied the correction curves and calibration factor obtained at all the observed spectra.

At the end we obtained 120 flux calibrated spectra for each galaxy.

We combined all the reduced data and finally we used the IRAF<sup>1</sup> task *apall*, with the aperture size of 5 pixel, to extract one-dimensional spectra for the objects. The list of the sample of galaxies selected for this project are listed in Table 4. The table lists the properties of the objects: ID, RA, DEC, R magnitude, spectroscopic redshift, signal to noise ratio of the summed spectra, stellar mass and gas phase metallicity.

Because of the low signal to noise ratio of some reduced data, we can not use all the spectra for our analysis. After a careful visual inspection, we removed from our sample the galaxy CDFS-5161 because its spectrum presents too low signal-to-noise ratio to detect the single lines. Moreover, we combined the three galaxies CDFS-12361, CDFS-9313, and CDFS-6664 in order to improve the signal of the single spectra (hereafter we call it CDFS-comb spectrum). The spectrum of the CDFS-4417 galaxy was good enough to be used individually.

<sup>1</sup> IRAF (Image Reduction and Analysis Facility) is distributed by the National Optical Astronomy Observatories, which are operated by the Association of Universities for Research in Astronomy, Inc., under co-operative agreement with the National Science Foundation.

**Table 4.** Properties of objects observed with FORS: Col. 1 object name in the MUSIC catalog (Grazian et al. 2006), Cols. 2,3, coordinates (J2000), Col. 4 R-band magnitude, Col. 5 spectroscopic redshift, Col. 6 the signal to noise ratio, Col. 7 Stellar Mass and Col. 8 gas metallicity.

ID	RA(J2000)	DEC(J2000)	Rmag	$z$	SNR <sup>a</sup>	$\text{Log}M$	$12 + \text{Log}(O/H)_{\text{gas}}$
CDFS-12631	03 32 18.1	-27 45 19.0	24.72	3.709	7	$9.84^{+0.15}_{-0.07}$	$8.22^{+0.18b}_{-0.14}$
CDFS-9313	03 32 17.2	-27 47 54.4	24.82	3.654	8	$9.34^{+0.17}_{-0.23}$	$7.95^{+0.25b}_{-0.23}$
CDFS-6664	03 32 33.3	-27 50 07.4	24.80	3.797	8	$8.98^{+0.20}_{-0.09}$	$7.63^{+0.23c}_{-0.29}$
CDFS-5161	03 32 22.6	-27 51 18.0	24.96	3.660	4	$9.73^{+0.22}_{-0.23}$	$7.69^{+0.23b}_{-0.38}$
CDFS-4417	03 32 23.3	-27 51 56.8	23.42	3.473	14	$10.38^{+0.15}_{-0.04}$	$8.55^{+0.09c}_{-0.10}$

**Notes.** <sup>(a)</sup> Signal-to-noise ratio in the wavelength used<sup>(b)</sup> Troncoso et al. in preparation <sup>(c)</sup> Maiolino et al. 2008.

### 3.3. Continuum level and EWs

Defining the continuum is a critical step in measuring the EWs. First, the signal-to-noise ratio of our spectra is generally limited (see Tab. 4) and changes significantly with wavelength because of the presence of sky-lines. Second, at our resolution most of the spectrum is affected by absorption lines. Taking into account these two problems, we fit the continuum by using a third- or fifth-order polynomial, depending on the continuum shape, by using only regions that are expected to be free from deep absorption lines. To define the continuum, we use the *Starburst99* spectra, excluding all the regions where absorption larger than 5% are expected for solar metallicities. This method defines a continuum which is slightly underestimated. The amount of correction needed can be measured by applying the same technique to theoretical spectra, where the continuum level is well known. We obtain that our fitting method defines a continuum level that is  $3\% \pm 2\%$  below the real one, depending on the spectrum used. This means that the continuum bias can be removed by multiplying the normalized spectra by 1.03. A series of simulations were also used to estimate the uncertainties on the continuum level in each target galaxy. Random gaussian noise was added to the *Starburst99* spectra to obtain the same signal-to-noise observed in each spectrum, and the continuum was fitted, repeating the procedure many times. We obtain that the continuum level is uncertain of about 5% for CDFS-4417, and 10% for the combined spectrum, and that this uncertainty is fairly constant with wavelength.

The EW are measured with respect to this fitted continuum, after excluding regions affected by bright sky lines. The uncertainties on the EWs derive from both the poisson noise on the used pixels, and on the uncertainties on the continuum level described above. The latter contribution is dominant in all cases, and can become very large for F1978 which is  $85\text{\AA}$  wide. On the contrary, F1501 index is defined on the narrowest wavelength range and is less affected by this contribution. As a result, usually F1501 is the most reliable index for our galaxies.

### 3.4. Results

The EWs measured as described above are compared with the calibrations in Tab. 2 to obtain the stellar metallicities. We will not consider neither F1370, which is not measurable in our spectra of limited signal-to-noise, nor F1978, which, for our redshifts, falls in wavelength regions covered

by many sky lines. Therefore for the observed galaxies we can use only F1425, F1460, and F1501.

Fig. 4 and Fig. 5 show the comparison of the observed spectrum of CDFS-4417 (solid line) and the composite spectrum CDFS-comb (solid line) with the theoretical model (dotted line), computed for five different metallicities for the indices considered to compute the stellar metallicity. Among the five models plotted in the figures, the metallicities that most closely match the observations are  $0.2Z_{\odot}$ , in all the spectra regions considered.

This agreement can be made more quantitative using the equations reported in Table 2 and computing the metallicity for the observed objects. In Table 5 we present the value found for each available features with the associated error calculated applying the theory of propagation of the error, i.e. we propagated the uncertainties both in the observations and the models to get the final value. The last column of the Table 5 represents the final value of metallicity from weighted average of the value of the single features and the associated weighted error.

Because in our spectra we did not observe any emission at  $1533\text{\AA}$ , we calculated the metallicity of the spectrum CDFS-4417 applying the Equation 2, and we found a value of  $Z = 0.26Z_{\odot} \pm 0.12$ . This value is in good agreement with what found using the other indicators ( $0.23 \pm 0.22$ ), and the associated formal error is lower. This suggests that it is possible to use the SiII at  $1533\text{\AA}$  as metallicity indicator when the spectra is free from the Si II\* fine-structure emission line. The final value of the stellar metallicity does not change even computing the weighted average using also this feature, where possible.

The gas phase metallicity of the CDFS-4417 was taken from Maiolino et al. (2008), while for the combined FORS spectrum we combined rest frame optical spectrum in the same way we did for the rest frame UV one, in order to derive consistent properties. We measured the gas phase metallicity with the  $R_{23}$  using the line fluxes measured on the combined spectrum.

## 4. Other data from literature

To enlarge the sample we collected from the literature other rest frame UV spectra suitable for this kind of work.

To compute the gas-phase metallicity we consider one of the most frequently used metallicity diagnostics, the  $R_{23}$  parameter, defined as:

$$R_{23} = \frac{F([\text{OII}]\lambda 3727) + F([\text{OIII}]\lambda 4959) + F([\text{OIII}]\lambda 5007)}{F(\text{H}\beta\lambda 4861)}$$



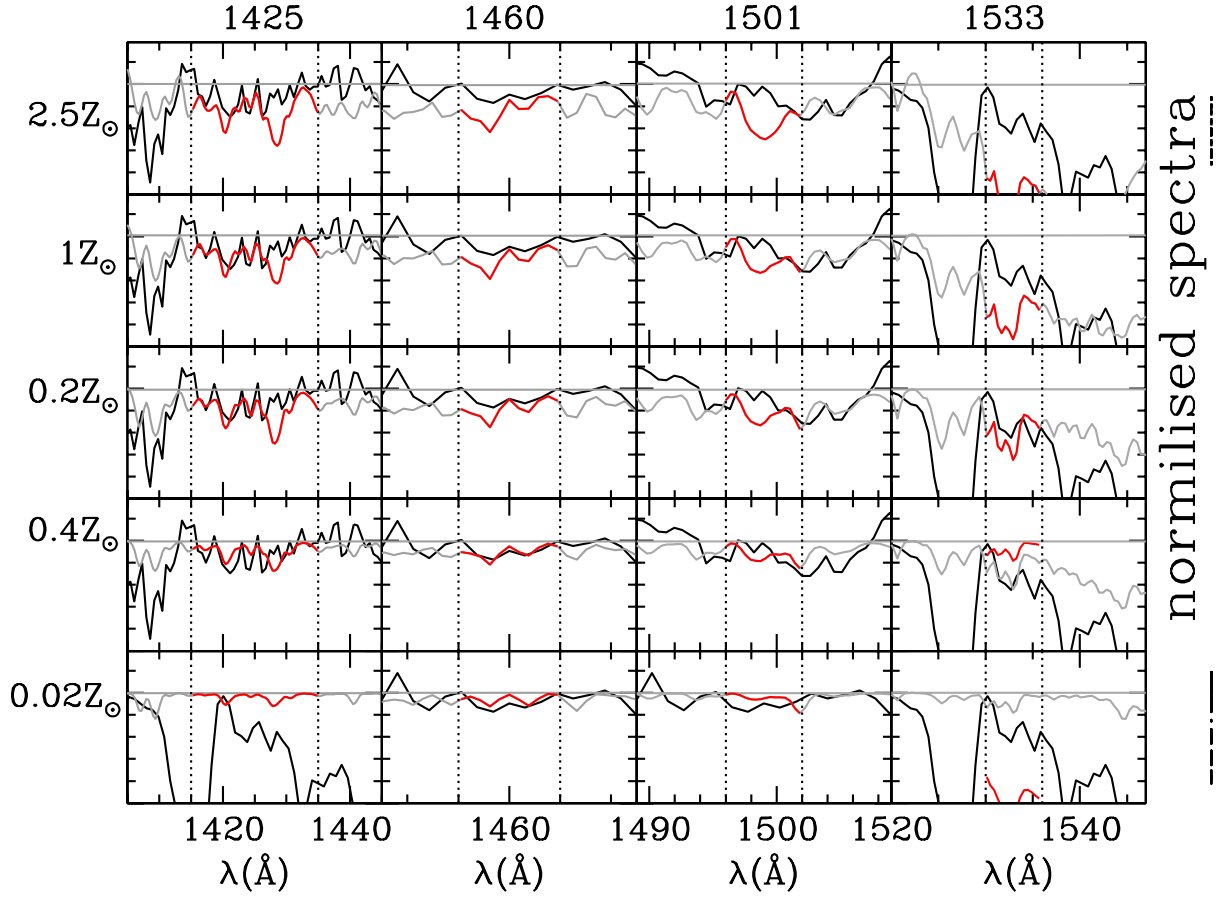


**Fig. 4.** Comparison of the observed spectrum of the object CDFS-4417 at  $z = 3.47$  (black line) with the theoretical spectra (dotted grey line) produced by *Starbursts99* for five different metallicities, for the each index used to compute the stellar metallicity. In red are highlighted the metallicity indicators. All the spectra are normalized by the fitted continuum.

**Table 5.** Metallicity measured in the observed galaxies with the errors computed used all the available indicator, and weighted average.

ID	F1425	F1460	F1501	Weighted Average
CDFS-4417	$0.14 \pm 0.44$	$0.17 \pm 0.47$	$0.30 \pm 0.32$	$0.23 \pm 0.22$
CDFS-comb	$0.13 \pm 0.74$	$0.37 \pm 0.62$	–	$0.24 \pm 0.45$

where  $F([\text{O II}]\lambda 3727)$ ,  $F([\text{O III}]\lambda 4959)$  and so on denote the emission-line fluxes of  $[\text{O II}]\lambda 3727$ ,  $[\text{O III}]\lambda 4959$  and so on, respectively. The  $R_{23}$  was proposed by Pagel et al. (1979), and its calibration to the oxygen abundance has been improved by both photoionization model calculations (e.g., McGaugh 1991; Kewley & Dopita 2002), and empirical calibrations (Nagao et al. 2006). For consistency with the FORS galaxies discussed above, and to compare with the data of Mannucci et al. (2010), we used the most recent  $R_{23}$  calibration provided by Maiolino et al. (2008).

#### 4.1. The Cosmic Horseshoe

The spectrum of Cosmic Horseshoe, a gravitationally lensed galaxy at  $z = 2.38$ , was analyzed by Quider et al. (2009). They measured the EW of the F1425 and following the definition and obtained the metallicity  $Z = 0.5Z_{\odot}$ . Their value

of the EW are obtained considering the pseudo continuum as defined in Rix et al. (2004). To make a consistent comparison of the Cosmic Horseshoes metallicity with the other galaxies, we measured the EWs using the definition of the real continuum described in 3.3, and computing the metallicity with the equation 1. With our procedure the metallicity found is  $Z = 0.37Z_{\odot}$ , i.e.  $12 + \log(\text{O}/\text{H}) = 8.26 \pm 0.29$ . For consistency, we recomputed the gas phase metallicity for this galaxies using the  $R_{23}$  index with the emission line fluxes taken from Hainline et al. (2009) and the metallicity calibration of Maiolino et al. (2008). In this way we obtained  $12 + \log(\text{O}/\text{H}) = 8.48 \pm 0.1$ .

We measured, for the first time, the stellar mass of the Cosmic Horseshoe. We obtained the IRAC photometry at  $3.6 \mu\text{m}$  and  $4.5 \mu\text{m}$  by using Spitzer archive images and using a photometric aperture of 8 arcsec and subtracting the flux from the central lensing galaxy. The U, G and I photometry were taken from Belokurov et al. (2007).

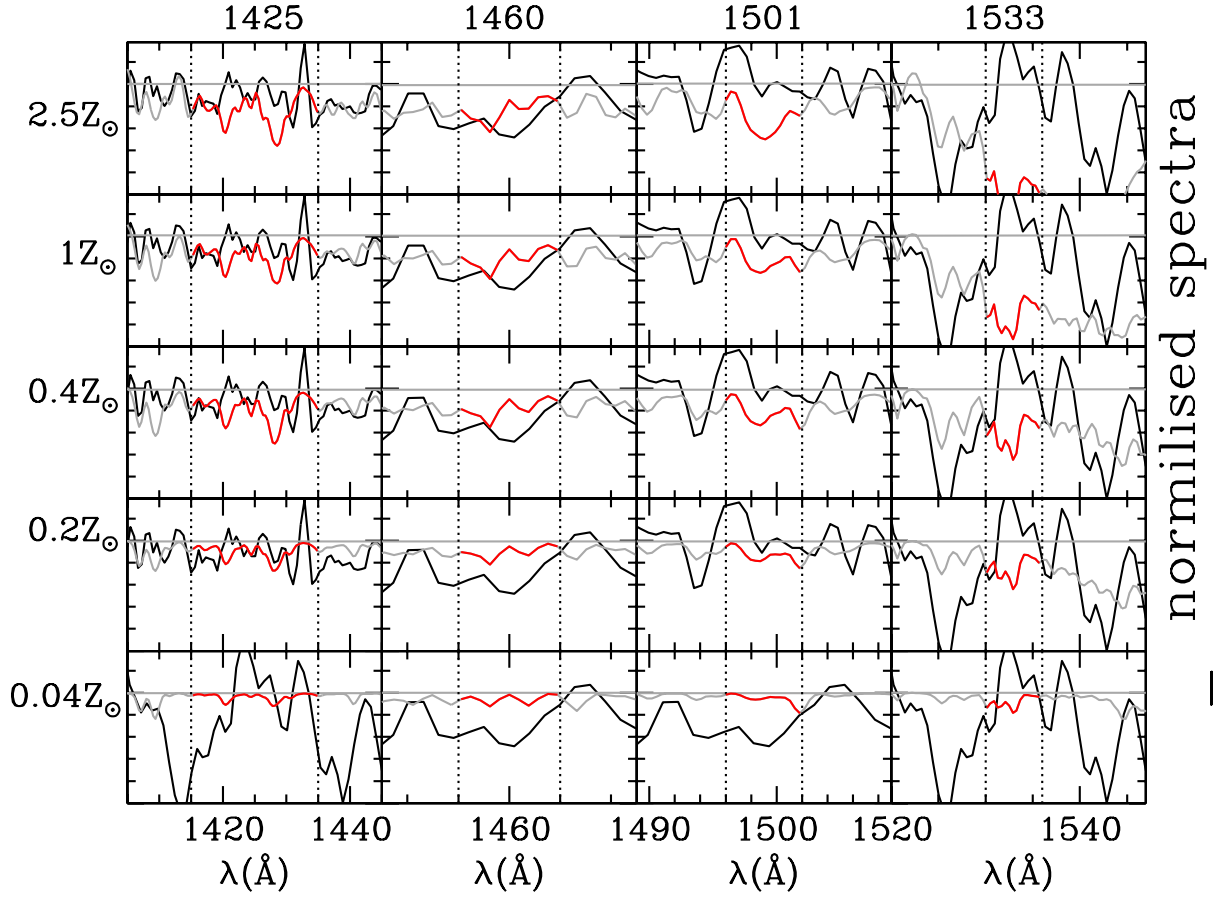


**Fig. 5.** Comparison of the observed combined spectrum of the object CDFS-comb at  $z = 3.71$  (black line) with the theoretical spectra (dotted grey line) produced by *Starburts99* for five different metallicities, for the each index used to compute the stellar metallicity. In red are highlighted the metallicity indicators. All the spectra are normalized by the fitted continuum.

We used the Hyperzmass code (Pozzetti et al. 2007 and Bolzanella et al. 2000), with Bruzual & Charlot (2003) libraries, assuming a Chabrier IMF (Chabrier et al. 2003) with an upper mass limit of  $100M_{\odot}$ , smooth exponentially decreasing Star Formation Histories (SFHs) with time scale  $\tau = [0.1, \infty]$  and age  $t = [0.1, 20]$ , deriving a mass of  $\text{Log}(M/M_{\odot}) = 10.56 \pm 0.19$ , corrected for the magnification.

#### 4.2. The Cosmic Eye

The lensed galaxy Cosmic Eye at  $z = 3.075$ , has been studied by Quider et al. (2010). They did not use the method explained by Rix et al. (2004) to compute the metallicity because of the heavy contamination of absorption lines in the region of the F1425 index that could compromise the definition of the continuum. They gave just an indication of the metallicity,  $Z \sim 0.40Z_{\odot}$ , comparing the observed spectrum with the models. Computing the EW of the other indices and applying our calibration, we found metallicity  $Z = 0.30Z_{\odot}$ , i.e.  $12 + \log(O/H) = 8.16 \pm 0.28$ .

The gas phase metallicity is  $12 + \log(O/H) = 8.60 \pm 0.11$ , computed taken the value of  $R_{23}$  from Stark et al. (2008) and applying it in the metallicity calibrations of Maiolino et al. (2008).

The stellar mass of the Cosmic Eye derived from SED fit-

ting is  $\text{Log}(M/M_{\odot}) = 9.55 \pm 0.14$  (Troncoso et al. in preparation).

#### 4.3. MS 1512-cB58

The last spectrum that we obtained belong to the MS 1512-cB58 (Pettini et al. 2000), a gravitational lensed galaxies at  $z = 2.72$  that, thanks to the magnification, presents a spectrum with very high signal to noise ratio. As for the previous galaxies, we measured the EWs for all the defined indicators on the spectra using the real continuum and we obtained a stellar metallicity from equation 1 of  $Z = 0.44Z_{\odot}$ , i.e.  $12 + \log(O/H) = 8.33 \pm 0.25$ .

To compute the gas phase metallicity we took the emission line fluxes in Teplitz et al. (2000), and applied the  $R_{23}$  calibration of Maiolino et al. (2008). The result is  $12 + \log(O/H) = 8.35 \pm 0.15$ .

The stellar mass of MS 1512-cB58 is  $\text{Log}(M/M_{\odot}) = 8.94 \pm 0.15$  (Siana et al. 2008).

#### 4.4. Other galaxies

For five additional high redshift galaxies it was not possible to obtain the spectra, but only the value of the EWs from the literature. This is the case of the lensed galaxy 8 o'clock arc at  $z = 2.73$  studied by Dessauges-Zavadsky et

al. (2010), as well as for the four galaxies of the Fors Deep Field with redshift  $2.3 < z < 3.5$  presented in Mehlert et al. (2006). Both these papers provide the F1425 index, as defined by Rix et al. (2004), based on the “pseudo continuum”.

For the lensed galaxy 8 o’clock arc we found that the stellar metallicity is  $Z = 0.52Z_{\odot}$ , i.e.  $12 + \log(O/H) = 8.40$ .

Again, to be consistent with the other results, the gas phase metallicity was computed with the  $R_{23}$  index with the emission line fluxes taken from Finkelstein et al. (2009) and using the calibrations of Maiolino et al. (2008). We obtained  $12 + \log(O/H) = 8.48 \pm 0.1$ .

The stellar mass of this galaxy is  $\text{Log}(M/M_{\odot}) = 10.25^{+2.22}_{-0.68}$  (Richard et al. 2011). We can not give the errors for the stellar metallicity of this galaxy because Dessauges-Zavadsky et al. (2010) did not give any indication of the uncertainties relative to the EWs measurements.

In the same way, we calculated the stellar metallicity for four FORS Deep Field galaxies studied by Mehlert et al. (2006). It was not possible to compute the gas phase metallicity because the emission line fluxes for these galaxies are not available. We reported the results in Fig. 7, where we highlighted these objects with black crosses. The masses of these galaxies were provided by Drory et al. (2005 and private communication).

## 5. Comparison between stellar and gas-phase metallicities

In this section we compare the stellar metallicity obtained using the empirical calibrations described above with the gas phase ones.

Small differences are expected between the stellar metallicities as measured using UV absorption features and the gas phase metallicities obtained by strong optical emission lines. Nevertheless, if the galaxy is experiencing a rapid metallicity evolution, differences could be related to the longer lifetimes of the star dominating UV emission with respect to the more massive stars dominating line emission. In fact, the stars responsible of the UV emission are young, hot O-B stars (with a life time of  $\sim 10^6 - 10^7$  yr), which were formed from interstellar gas with very similar properties of the one seen in emission given their short lifetime.

On the other hand, larger differences are expected using optical absorption features, dominated by longer lived stars (e.g. Lick indices, as found in Galazzi et al. (2005) and Panter et al. (2008) for local SDSS galaxies).

In Table 6 we report the comparison between stellar and gas phase metallicity for the objects that we discussed in the previous sections. The differences between the stellar and the gas-phase metallicity are plotted in Fig. 6. For each galaxies the error are computed by combining the errors from the gas-phase and stellar metallicities in quadrature.

As expected, we do not find large discrepancy between the two quantities: the average difference is -0.16 and the uncertainty is 0.14, therefore the difference has a significance of about 1.1sigma. This does not allow us to claim any significant difference, given the large systematic uncertainties associated with both methods. Also Halliday et al. (2008), analyzing star forming galaxies at  $z \sim 2$  found the stellar metallicity lower by  $\sim 0.25\text{dex}$  than the gas phase one measured for galaxy with similar stellar mass and redshift. It is worth noticing that, since Halliday et al. (2008)

are not comparing the metallicities of the same galaxies, some selection effects present in one or both data sets could affect the results. To verify if any difference is real larger sample of galaxies are clearly needed.

## 6. The stellar mass-metallicity relation

Our data allow for the first time the study of the stellar mass-metallicity relation at high redshift.

Fig. 7 shows the position and the relative error of the observed galaxies (black squares) at  $z > 3$  presented above in the MZ-plane. The black triangles represent the stellar metallicity for the lensed galaxies. The black crosses are the stellar metallicity calculated for galaxies at  $z \sim 3$  taken by Mehlert et al. (2006). All the quantities are computed in the same way and are consistent.

To compare our finding with the previous studies, in the Fig. 7 we draw the various mass-metallicity relations found at different redshifts both for stellar and gas phase metallicity. For the latter, the black dotted line is the relation obtained by Tremonti et al. (2004) in the local universe as derived from the the SDSS, at  $z \sim 0.07$ , the magenta dotted line represents the relation obtained by Erb et al. (2006) at  $z \sim 2.2$ , and the blue dotted line shows the behavior of such relation inferred from the initial sample of LSD and AMAZE sources at  $z \sim 3$  by Mannucci et al (2009).

The green dotted line in Fig. 7 represents the stellar metallicity relation found by Panter et al. (2008) for local SDSS galaxies.

As discussed in the previous section, the derived stellar metallicities are consistent, although slightly lower, than the gas phase ones. The stellar metallicities therefore provide an independent test of the reliability of the metal abundances in high redshift galaxies, more often obtained for the gas phase only using strong optical emission line ratios. In fact, the strong line diagnostics used are indirect tracers, calibrated in local galaxies, and depend not only on metallicity, but also on other parameters as ionization conditions and densities, which might in principle be very different in high- $z$  star forming galaxies than in local spirals (see e.g. Nagao et al. 2006, Brinchmann et al. 2008). Our result therefore confirms the low chemical abundances derived from optical line ratios at high redshift, and the strong evolution in gas phase and young stars metallicity with respect to local and lower redshift galaxies, as already claimed by Maiolino et al. (2008) and Mannucci et al. (2009). Although the large uncertainties in both stellar and gas-phase metallicity measurements, it additionally support the finding of Mannucci et al (2010) and Troncoso et al. (in prep.) that the Fundamental Metallicity Relation between mass, metallicity and SFR is evolving at  $z \sim 3$ , while no evolution is found at lower redshifts (see also Cresci et al. 2011).

As shown in Fig. 6, the stellar metallicities derived for  $z \sim 3$  galaxies are comparable with the ones obtained by Galazzi et al. (2005) and Panter et al. (2008) for local SDSS galaxies. However the stellar populations that are dominating the spectral features considered in the two cases to compute the metallicity are different: in fact, in high redshift galaxies the rest frame UV spectrum that we observe is dominated by hot, young stellar populations, while in the local universe the optical indices used by Panter et al. (2008) are dominated by cold, older stars: as noted by

**Table 6.** Comparison between the stellar metallicity obtained with this work and gas phase metallicity. In all the cases we assume a solar value of  $\log(Z/Z_{\odot} = 12 + \log(O/H) - 8.69$  (Allende Prieto et al. 2001). The Mass is  $\log(M/M_{\odot})$ .

ID	Mass	redshift	stellar metallicity	gas metallicity
CDFS-4417	10.38	3.47	$8.05 \pm 0.22$	$8.46 \pm 0.11^{(a)}$
CDFS-comb	9.38	3.71	$7.92 \pm 0.24$	$7.98 \pm 0.15^{(b)}$
horseshoe	10.56	2.37	$8.26 \pm 0.29$	$8.48 \pm 0.11^{(c)}$
8oclock	10.25	2.73	$8.40 - - -$	$8.42 \pm 0.10^{(d)}$
Cosmic eye	9.60	3.07	$8.36 \pm 0.20$	$8.60 - - -^{(b)}$
MS 1525 cB58	8.94	2.72	$8.33 \pm 0.25$	$8.35 \pm 0.15^{(e)}$
FDF-3173	9.96	3.27	$8.54 - - -$	$- - - - -$
FDF-3810	10.95	2.37	$8.90 - - -$	$- - - - -$
FDF-5903	11.01	2.77	$8.24 - - -$	$- - - - -$
FDF-6934	11.31	2.44	$8.57 - - -$	$- - - - -$

**Notes.** The gas metallicity was calculated using the calibration of Maiolino et al. (2008), and the emission line fluxes taken from <sup>(a)</sup> Maiolino et al. (2008) <sup>(b)</sup> Troncoso et al. in prep. <sup>(c)</sup> Hainline et al. (2009) <sup>(d)</sup> Finkelstein et al. (2009) <sup>(e)</sup> Teplitz et al. (2000). respectively.

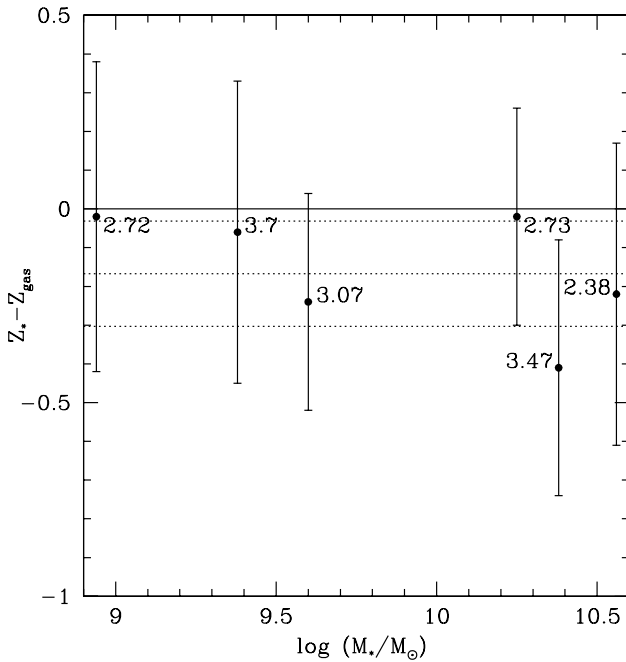


**Fig. 6.** Difference between the stellar and the gas-phase metallicity of the galaxies. The redshift of each source is reported in the labels. The dotted lines are the mean value of the differences and the  $1-\sigma$  deviation.

Panther et al. (2008), their stellar metallicities for the galaxies with a younger stellar populations ( $\leq 1$  Gyr) are better in agreement with the gas phase ones, while larger deviations are present for the galaxies dominated by an older population. Therefore, a direct, straightforward comparison of the two is not possible. However, the fact that the stellar metallicities of the SDSS sample are comparable with both gas phase and stellar abundances at  $z > 2.5$  is an indication that the bulk of the stellar populations in the galaxies investigated by Panther et al. (2008) were formed during this epoch.

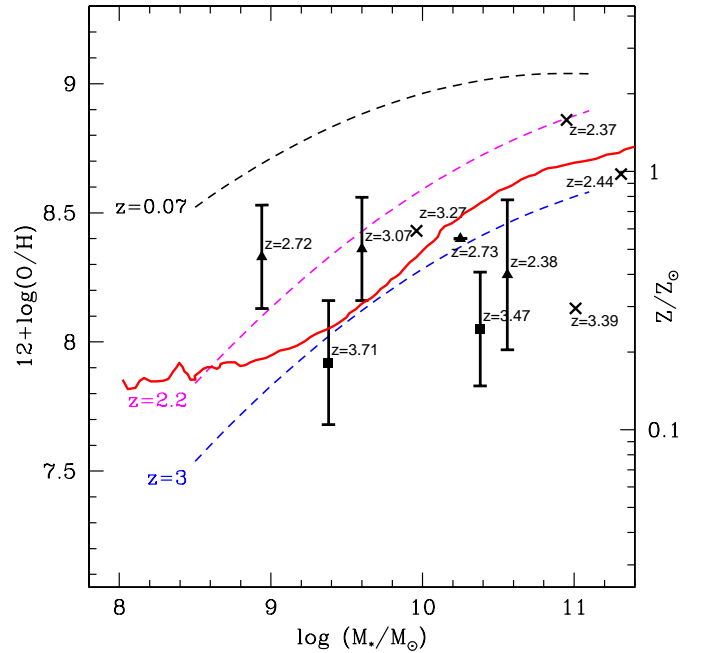


**Fig. 7.** Stellar mass-metallicity relation for the FORS galaxies at  $z \sim 3.3$  discussed in this work (black squares). The black triangles represent the stellar metallicity for the lensed galaxies from the literature (see text), and the black crosses are the stellar metallicity for the galaxies at  $z \sim 3$  taken by Meheert et al. (2006). For comparison, we draw the mass-metallicity relations for the gas component: the black line is the MZR obtained by Tremonti et al. (2004) at  $z = 0.07$ , the magenta line was found by Erb et al. (2006) at  $z = 2$ , and the blue dotted line shows the relation from the LSD and AMAZE inferred by Mannucci et al. (2009) at  $z \sim 3.5$ . The red line is stellar mass-metallicity relation found by Panther et al. (2008) in local universe.

## 7. Conclusions

In this paper, we have investigated for the first time the stellar mass-metallicity relation at high redshift,  $z \sim 3$ . Using the theoretical spectra created with the population synthesis code *Starbursts99*, we looked for photospheric ab-

sorption lines to be used as indicators of stellar metallicity. First we tested the line indices proposed by Leitherer et al. (2001) and Rix et al. (2004), the F1370, F1425 and F1978 using the last version of *Starbursts99*, although the F1978 shows a strong dependence from the resolution and the IMF.

Then we defined two new photospheric lines, F1460 and F1501, and we found that these lines are sensitive to the metallicity and almost independent of the age and the IMF, and therefore useful stellar metallicity indicators. The F1501 index seems to be the most promising because it is defined on the narrowest wavelength range and less affected by the uncertainties on the continuum definition. We provided the metallicity calibrations, see Fig. 3, with two different definitions of the continuum: the first relations are referred to the real continuum, that we suggest to use in case of spectra with low signal-to-noise ratio, the others were obtained using the definition of the “pseudo-continuum” provided by Rix et al. (2004), that we recommend in case of high signal-to-noise spectra, see Sec. 2.3.

We applied the relations on one galaxy and a composite spectra comprised of three additional galaxies of the AMAZE sample at  $z \sim 3.3$ , for which the gas phase metallicity and the galaxy masses were already known.

We took from the literature the spectra of eight additional galaxies, and we recompute their stellar metallicity using the new calibrations.

At the end we compared the results found with the gas phase metallicity for each object, see Fig. 6. The main conclusion of this work is that within the errors, the stellar and the gas phase metallicity are consistent, although there seems to be a tendency to find stellar metallicity lower than the gas phase one by  $\sim 0.1dex$ , as already found by Halliday et al. (2008). This result supports the low metal content derived for the gas phase of high- $z$  galaxies from optical strong line ratios, as well as an evolution of the Fundamental Metallicity Relation at  $z > 3$  as found by Mannucci et al. (2010).

For the first time, we obtained the stellar mass-metallicity at redshift  $z > 2.5$ , see Fig. 7. We notice that the stellar metallicities found at high redshift is comparable with those found by Panter et al. (2008) for local galaxies, although the two are not straightforwardly comparable as in high redshift galaxies the stellar metallicity are computed for hot, young stars, while in the local galaxies for cold, older stellar population.

In summary, the rest-frame UV is rich in metallicity dependent features, which are able to provide a measure of stellar metallicity in high redshift galaxies. This represent an independent measure of the chemical abundances in galaxies with respect to the more widespread gas phase metallicities, which can provide important constraints to the star formation histories of galaxies in the early Universe. Although this technique is currently limited to very bright or lensed galaxies by the high S/N required, the advent of next generation of telescopes will give us much higher quality spectra for high redshift galaxies, and the stellar metallicity indicators will play a more important role in chemical abundances studies at high redshift.

*Acknowledgements.* GC acknowledges financial support from ASI-INAf grant I/009/10/0. Thanking Chuck Steidel for his spectrum of MS1512-cB58, and Alice Shapley for her spectra of some lensed galax-

ies. We thank Max Pettini and Claus Litherer for useful comment and suggestions. We are grateful to Drory for providing the masses of the FDF galaxies.

## References

- Appenzeller, I., Duensing, K. H., Fricke, K., Gong, S., Hess, H.-J., et al., 1992, *ESOC*, 42, 577
- Belokurov, V., Evans, N. W., Moiseev, A., King, L. J., Hewett, P. C., et al., 2007, *ApJ*, 671, 9
- Bolzonella, M., Miralles, J.-M., & Pell, R., 2000, *A&A*, 363, 476
- Bresolin, F., Pietrzyski, G., Urbaneja, M. A., Gieren, W., Kudritzki, R.-P., & Venn, K. A., 2006, *ApJ*, 648, 1007
- Brinchmann, J., Pettini, M., & Charlot, S., 2008, *MNRAS*, 385, 769
- Brooks, A. M., Govervato, F., Booth, C. M., Willman, B., Gardner, J. P., Wadsley, J., Stinson, G., & Quinn, T., 2007, *ApJ*, 655, L17
- Bruzual, G., & Charlot, S., 2003, *MNRAS*, 344, 1000
- Calura, F., Pipino, A., Chiappini, C., Matteucci, F., & Maiolino, R., 2009, *A&A*, 504, 373
- Campisi, M. A., Tapparello, C., Salvaterra, R., Mannucci, F., & Colpi, M., 2011, *MNRAS*, 1437
- Chabrier, G., 2003, *ApJ*, 586, 133
- Cresci, G., Mannucci, F., Maiolino, R., Marconi, A., Gnerucci, A., & Magrini, L., 2010, *Nature*, 467, 811
- Cresci, G., Mannucci, F., Sommariva, V., Maiolino, R., Marconi, A., et al., 2011, *arXiv1110.4408*
- Contini, T., Epinat, B., Queyrel, J., Vergani, D., Tasca, L., et al., 2011, *arXiv1103.5579C*
- Dayal, P., Ferrara, A., Saro, A., Salvaterra, R., Borgani, S., & Tornatore, L., 2009, *MNRAS*, 400, 2000
- Davé, R., Finlator, K., & Oppenheimer, B. D., 2007, *EAS*, 24, 183
- Davé, R., Finlator, K., Oppenheimer, B. D., 2011, *MNRAS*, 416, 135
- Dessauges-Zavadsky, M., D’Odorico, S., Schaerer, D., Modigliani, A., Tapken, C., et al., 2010, *A&A*, 510, 26
- Dekel, A., & Woo, J., 2003, *MNRAS*, 344, 1131
- de Mello, D. F., Leitherer, C., & Heckman, T. M., 2000, *ApJ*, 530, 251
- de Rossi, M. E., Tissera, P. B., & Scannapieco, C., 2007, *MNRAS*, 374, 323
- Drory, N., Salvato, M., Gabasch, A., Bender, R., Hopp, U., et al., 2005, *ApJ*, 619, 131
- Ellison, S. L., Patton, D. R., Simard, L., & McConnachie, A. W., 2008, *ApJ*, 672L, 107
- Erb, D. K., Steidel, C. C., Shapley, A. E., Pettini, M., Reddy, N. A., et al., 2006, *ApJ*, 646, 107
- Erb, D. K., 2008, *ApJ*, 674, 151
- Erb, D. K., Pettini, M., Shapley, A. E., Steidel, C. C., Law, D. R., et al., 2010, *ApJ*, 719, 1168
- Feulner, G., Gabasch, A., Salvato, M., Drory, N., Hopp, U., et al., 2005, *ApJ*, 633, L9
- Finlator, K., & Davé, R., 2008, *MNRAS*, 385, 2181
- Finkelstein, S. L., Papovich, C., Rudnick, G., Egami, E., Le Floch, E., et al., 2009, *ApJ*, 700, 376
- Gallazzi, A., Charlot, S., Brinchmann, J., & White, S. D. M., 2006, *MNRAS*, 370, 1106
- Garnett, D. R., 2002, *ApJ*, 581, 1019
- Garnett, D. R., Kennicutt, R. C., & Bresolin, F., 2004, *ApJ*, 607L, 21
- Grazian, A., Fontana, A., de Santis, C., Nonino, M., Salimbeni, S., et al., 2006, *A&A*, 449, 951
- Hainline, K. N., Shapley, A. E., Kornei, K. A., Pettini, M., Buckley-Geer, E., et al., 2009, *ApJ*, 701, 52
- Halliday, C., Daddi, E., Cimatti, A., Kurk, J., Renzini, A., et al., 2008, *A&A*, 479, 417
- Juneau, S., Glazebrook, K., Crampton, D., McCarthy, P. J., Savaglio, S., et al., 2005, *ApJ*, 619, L135
- Kewley, L. J., Dopita, M. A., 2002, *ApJ*, 201, 1406
- Kewley, L. J., & Ellison, S. L., 2008, *ApJ*, 681, 1183
- Kobulnicky, H. A., & Skillman, E. D., 1996, *ApJ*, 471, 211
- Kppen, J., Weidner, C., & Kroupa, P., 2007, *MNRAS*, 375, 673
- Kobayashi, C., Springel, V., & White, S. D. M., 2007, *MNRAS*, 376, 1465
- Leitherer, C., & Heckman, T. M., 1995, *apJS*, 96, 9L
- Leitherer, C., Schaerer, D., Goldader, J. D., Gonzalez, D., Rosa, M., et al., 1999, *ApJ*, 123, 3
- Leitherer, C., Leo, J. R. S., Heckman, T. M., Lennon, D. J., Pettini, M., & Robert, C., 2001, *ApJ*, 550, 724

- Leitherer, C., Ortiz Otlvaro, P. A., Bresolin, F., Kudritzki, R.-P., Lo Faro, B., Pauldrach, A. W. A., Pettini, M., & Rix, S. A., 2010, *ApJ*, 189, 309
- Liu, X., Shapley, A. E., Coil, A. L., Brinchmann, J., & Ma, C.-P., 2008, *ApJ*, 678, 758
- Mannucci, F., Cresci, G., Maiolino, R., Marconi, A., Pastorini, G., et al., 2009, *MNRAS*, 398, 1915
- Mannucci, F., Cresci, G., Maiolino, R., Marconi, A., Gnerucci, A., 2010, *MNRAS*, 408, 2115
- Mannucci, F., Salvaterra, R., & Campisi, M. A., 2011, *MNRAS*, 414, 1263
- Maier, C., Meisenheimer, K., & Hippelein, H., 2004, *A&A*, 418, 475
- Maiolino, R., Nagao, T., Grazian, A., Cocchia, F., Marconi, A., Mannucci, F., et al., 2008, *A&A*, 488, 463
- Mehlert, D., Tapken, C., Appenzeller, I., Noll, S., de Mello, D., et al., 2006, *A&A*, 455, 835
- Mouchine, M., Gibson, B. K., Renda, A., & Kawata, D., 2008, *ArXiv e-prints*
- Murray, N., Quataert, E., & Thompson, Todd A., 2005, *ApJ*, 618, 569
- Nagamine, K., Fukugita, M., Cen, R., Ostriker, J. P., 2001, *MNRAS*, 558, 479
- Nagao, T., Maiolino, R., & Marconi, A., 2006, *A&A*, 459, 85
- Nakajima, K., et al. 2011, *asXiv:1105.2824*
- Oppenheimer, B. D., & Davé, Romeel, 2008, *MNRAS*, 387, 577
- Panter, B., Jimenez, R., Heavens, A. F., & Charlot, S., 2008, *MNRAS*, 391, 111
- Pettini, M., Ellison, S. L., Steidel, C. C., & Bowen, D. V., 1999, *ApJ*, 510, 576
- Pettini, M., Steidel, C. C., Adelberger, K. L., Dickinson, M., & Giavalisco, M., 2000, *ApJ*, 528, 96
- Pettini, M., Shapley, A. E., Steidel, C. C., Cuby, J.-G., et al., 2001, *ApJ*, 554, 981
- Pettini, M., & Pagel, B., E.J., 2004, *MNRAS*, 348L, 49
- Pozzetti, L., Bolzonella, M., Lamareille, F., Zamorani, G., Franzetti, P., et al., 2007, *A&A*, 474, 443
- Quider, A. M., Pettini, M., Shapley, A. E., & Steidel, C. C., 2009, *MNRAS*, 398, 1263
- Quider, A. M., Shapley, A. E., Pettini, M., Steidel, C. C., & Stark, D. P., 2010, *MNRAS*, 402, 1467
- Richard, J., Jones, T., Ellis, R., Stark, D. P., Livermore, R., et al., 2011, *MNRAS*, 416, 463
- Rix, S. A., Pettini, M., Leitherer, C., Bresolin, F., Kudritzki, R.-P., & Steidel, C. C., 2004, *ApJ*, 615, 98
- Sanders, N. E., Soderberg, A. M., Valenti, S., Chomiuk, L., et al., 2011, *arXiv1110.23635*
- Salvaterra, R., Ferrara, A., & Dayal, P., 2010, *arXiv1003.3873*
- Sakstein, J., Pipino, A., Devriendt, J. E. G., & Maiolino, R., 2011, *MNRAS*, 410, 2203
- Savaglio, S., Glazebrook, K., Le Borgne, D., Juneau, S., Abraham, R. G., et al., 2005, *ApJ*, 635, 260
- Siana, B., Teplitz, H. I., Chary, R.-R., Colbert, J., & Frayer, D. T., 2008, *ApJ*, 689, 59
- Shapley, A. E., Steidel, C. C., Pettini, M., & Adelberger, K. L., 2003, *ApJ*, 588, 65
- Shapley, A. E., Coil, A. L., Ma, C.-P., & Bundy, K., 2005, *ApJ*, 635, 1006
- Shapley, A. E., 2011, *ARA&A*, 49, 525
- Somerville, R. S., Hopkins, P. F., Cox, T. J., Robertson, B. E., & Hernquist, L., 2008, *MNRAS*, 391, 481
- Spitoni, E., Calura, F., Matteucci, F., & Recchi, S., 2010, 514, 73
- Stark, D. P., Swinbank, A. M., Ellis, R. S., Dye, S., Smail, I. R., et al., 2008, *Nature*, 455, 755
- Stasiska, G., 2005, *A&A*, 434, 507
- Tassis, K., Kravtsov, A. V., & Gnedin, N. Y., 2008, *ApJ*, 672, 888
- Teplitz, H. I., McLean, I. S., Becklin, E. E., Figer, D. F., Gilbert, A. M., et al., 2000, *ApJ*, 533, 65
- Tissera, P., B., De Rossi, M., E., & Scannapieco, C., 2005, *MNRAS*, 364L, 38
- Tornatore L., Borgani S., Dolag K., & Matteucci F., 2007, *MNRAS*, 382, 1050
- Tremonti, C. A., Heckman, T. M., Kauffmann, G., Brinchmann, J., et al. 2004, *ApJ*, 613, 898
- Veilleux, S., Cecil, G., & Bland-Hawthorn, J., 2005, *ARAA*, 43, 769
- Weiner, B. J., Coil, A. L., Prochaska, J. X., Newman, J. A., et al., 2008, *ApJ*, 692, 187
- Yates, R. M., Kauffmann, G., & Guo, Q., 2011, *arXiv:1107.3145*
- Zahid, H. J., Kewley, L. J., & Bresolin, F., 2011, *ApJ*, 730, 137